Citation: Clin Transl Sci (2019) 12, 617–624; doi:10.1111/cts.12664

ARTICLE

A Physiologically-Based Pharmacokinetic Model for Targeting Calcitriol-Conjugated Quantum Dots to Inflammatory Breast Cancer Cells

James Forder[1], Mallory Smith[1], Margot Wagner[1], Rachel J. Schaefer[2], Jonathon Gorky[3], Kenneth L. van Golen[2], Anja Nohe[2] and Prasad Dhurjati[1,*]

Quantum dots (QDs) conjugated with 1,25 dihydroxyvitamin D3 (calcitriol) and Mucin-1 (MUC-1) antibodies (SM3) have been found to target inflammatory breast cancer (IBC) tumors and reduce proliferation, migration, and differentiation of these tumors in mice. A physiologically-based pharmacokinetic model has been constructed and optimized to match experimental data for multiple QDs: control QDs, QDs conjugated with calcitriol, and QDs conjugated with both calcitriol and SM3 MUC1 antibodies. The model predicts continuous QD concentration for key tissues in mice distinguished by IBC stage (healthy, early-stage, and late-stage). Experimental and clinical efforts in QD treatment of IBC can be augmented by *in silico* simulations that predict the short-term and long-term behavior of QD treatment regimens.

Study Highlights

WHAT IS THE CURRENT KNOWLEDGE ON THE TOPIC?
☑ Recent studies have indicated that calcitriol has beneficial effects against SUM149 inflammatory breast cancer (IBC) proliferation, migration, and differentiation. Although preliminary studies on calcitriol-conjugated quantum dots (QDs) injected into mice with IBC have been encouraging, no model exists to predict the distribution of these QDs.

WHAT QUESTION DID THIS STUDY ADDRESS?
☑ The study addresses the parameters, connectivity, and mathematical relationships needed to construct a model to predict dynamic QD distribution in mice with IBC.

WHAT DOES THIS STUDY ADD TO OUR KNOWLEDGE?
☑ A physiologically-based pharmacokinetic model framework has been constructed and validated for multiple QDs, notably SM3 calcitriol QDs. Continuous QD concentration estimates for key tissues can be generated, with the ability for adjustments to cover a broad range of patient characteristics.

HOW MIGHT THIS CHANGE CLINICAL PHARMACOLOGY OR TRANSLATIONAL SCIENCE?
☑ The PBPK model provides a framework to guide or complement both experimental and clinical endeavors in QD treatment of IBC and to infer behavior of experiments not performed. With additional data, the model has the potential to provide further mechanistic understanding of the disease.

Inflammatory breast cancer (IBC) is an aggressive form of cancer, which makes up ~ 1–5% of breast cancer cases but accounts for 10% of breast cancer deaths annually in the United States.[1] Often, this form of cancer is difficult to diagnose and is typically not recognized until it has progressed to stage III or IV.[1] The median survival time after diagnosis is <15 months with recurrence rates as high as 50%.[2] Traditional treatment plans consisting of surgery and localized radiotherapy result in a <5% survival rate beyond 5 years, the lowest survival rate of any breast cancer subtype.[2] With more advanced treatment combining multiple-targeting approaches, IBC still only has 5-year and 10-year disease-free survival rates of <45% and 20%, respectively.[2]

IBC is a rapidly progressing and highly metastatic disease with a younger age of onset relative to other types of breast cancer.[2] Typical symptoms include erythema, edema, and thickening or pitting of the breast, which is caused by tumor emboli blocking dermal lymph drainage.[3] By the time discernable symptoms are present, IBC is already locally advanced as the breast cancer cells have grown into surrounding structures and sometimes to distant metastasis sites, commonly in the bone, lungs, and skin.[4,5] These nonspecific symptoms, especially in absence of the stereotypical lump formation, are often misidentified as an infection or rash leading to IBC being misdiagnosed as mastitis or generalized dermatitis, delaying the treatment of the underlying cancer.[1,2] As a result, when diagnosed with IBC, almost

[1]Chemical and Biomolecular Engineering, University of Delaware, Newark, Delaware, USA; [2]Biological Sciences, University of Delaware, Newark, Delaware, USA; [3]Daniel Baugh Institute for Functional Genomics and Computational Biology, Thomas Jefferson University, Philadelphia, Pennsylvania, USA. *Correspondence: Prasad Dhurjati (dhurjati@udel.edu)
Received: April 26, 2019; accepted: May 17, 2019. doi:10.1111/cts.12664

all women are lymph node–positive with approximately one-third having distant metastases.[2]

Current treatment involves a multiple-targeting approach due to the aggressive nature of IBC. Hormone treatment is ineffective for many patients with IBC because approximately one-third of IBC diagnoses are triple-negative.[1,2] Instead, current treatment plans involve systemic chemotherapy followed by a mastectomy to remove the tumor and surrounding tissue and finally localized radiotherapy.[1,2] In addition to this, patients with IBC are often prescribed vitamin D supplements due to the vitamin's beneficial effect on reducing the cancer's metastasis rate.[6] Despite this multimodality treatment plan, prognosis for patients with IBC is poor. Researchers are pursuing an improved treatment method for IBC, ideally one that could prevent tumor cell migration as well as preventing or disrupting the formation of tumor emboli.[2]

A potential new therapeutic is the active form of vitamin D, 1,25 dihydroxyvitamin D3 (calcitriol). Calcitriol is known to modulate calcium and phosphate homeostasis to maintain bone health; it is most biologically active in tissues positive for vitamin D receptors, including organs, such as the kidney and intestines, as well as bone and the parathyroid gland.[7,8] Recently, vitamin D has been demonstrated to be a regulator of breast cancer cell proliferation, invasion, migration, differentiation, and apoptosis *in vitro*. The antiproliferative effects are thought to be a result of calcitriol blocking the mitogenic effects of insulin-like growth factor I through downregulation of its receptors, causing the G1 phase of the cell cycle to pause.[9] In addition, it was found that SUM149 cells exposed to calcitriol exhibited a decreased ability to migrate, invade, and form tumor emboli, leading to decreased metastasis *in vivo*.[10,11] However, previous studies have required toxic dosages of calcitriol (over 0.50 μg) to have a significant effect, which would lead to hypercalcemia.[10–12] Therefore, targeting methods are required to reach desired levels of calcitriol at treatment sites without having an excess of calcitriol in the rest of the body.

Quantum dots (QDs) conjugated to calcitriol have previously been used to examine the distribution of calcitriol both *in vitro* and *in vivo*.[10,11] QDs are semiconductor nanoparticles around 15 nm in diameter, which can be used for fluorescent imaging under UV light and have a variety of surface chemistries that are compatible with living systems. They localize in the liver, lymph nodes, kidneys, and spleen in mice, with some effects on distribution from the polymer surface chemistry (conjugated with carboxyl groups in this case).[10] To use calcitriol QDs for direct imaging of live cells, QDs are conjugated to calcitriol using an esterification reaction to produce calcitriol QDs (CalQDs).[10,11] To avoid hypercalcemia and potential toxicity, these CalQDs can be manipulated to target tumor sites. Unlike other forms of breast cancer, IBC cells overexpress a hypoglycosylated form of Mucin-1 (MUC1), a glycoprotein that is expressed on the apical surface of epithelial cells. Recently, Schaefer *et al*.[10,11] have proposed a therapeutic method conjugating SM3 MUC1 antibodies with CalQDs (SM3 CalQDs). In their studies, Schaefer *et al*.[10,11] used florescent imaging to measure the accumulation of SM3 CalQDs in various organs as well as tumor tissue in mice with SUM149 IBC tumors. The SM3 CalQDs were shown to target MUC1 overexpressing IBC cells, identify localization of IBC tumor emboli, and act as a vehicle to administer calcitriol more directly to affected areas, mitigating hypercalcemia and other negative side effects.

To better elucidate the details of the distribution of SM3 CalQDs as well as finding an adequate dosing regimen, we look to create a physiologically-based pharmacokinetic (PBPK) model. However, one of the challenges in creating a model that demonstrates the distribution of SM3 CalQDs is capturing physiological differences due to the extent of tumor growth. In the early stages of IBC, the cancer cells are localized within the breast tissue. During the course of the disease, 70% of patients with IBC develop a distant metastasis, suggesting the need to model different dynamics for early-stage compared to late-stage IBC.[2] Additionally, acute inflammatory response to cancer can cause the spleen to become enlarged.[13] To demonstrate the dynamics of SM3 CalQDs in both early and late-stage cancer as well as a healthy mouse, three distinct models will be created characteristic of each stage.

METHODS

PBPK model

This PBPK model for the distribution of CalQDs in mice for use in IBC treatment is based on *a priori* physical laws and parameters. The organs included are those most relevant to CalQD distribution during the particular cancer phase being modeled. In both early-stage and late-stage cancer models, the plasma compartment behaves as the central compartment by which the QDs are carried to and from the other tissues. The treatment is modeled as an intravenous injection, so the substance is directly inserted into the plasma compartment as system input. The lungs, spleen, liver, and kidneys are included as they are richly perfused organs and have been shown to preferentially accumulate the QDs tested by Schaefer *et al*.[8,10,12] As IBC generates a large immune response, the spleen compartment is also used to model the influence of splenomegaly often seen in patients with cancer. The liver receives blood flow from the spleen and is vital for clearance and breakdown of the CalQDs in the body via biliary secretion.[14,15] Additionally, the lungs are one of the most common sites for early IBC metastasis. Previous studies have shown that QDs injected intravenously in mice localize in the liver, kidneys, and spleen.[10,14] The "other" compartment was included as a lumped compartment for tissues not explicitly mentioned.

In late-stage models, a tumor compartment is included in parallel to the other organs to represent delocalized tumor tissue throughout the body due to metastasized tumors. In contrast, in the early-stage model, a tumor is housed in a compartment parallel to the breast so that it is surrounded by breast tissue. These organs were connected according to their vascular connections in the human body (**Figure 1**).

Assumptions

The concentration of CalQDs in each compartment in the model was based on the dynamics of a continuous-stirred

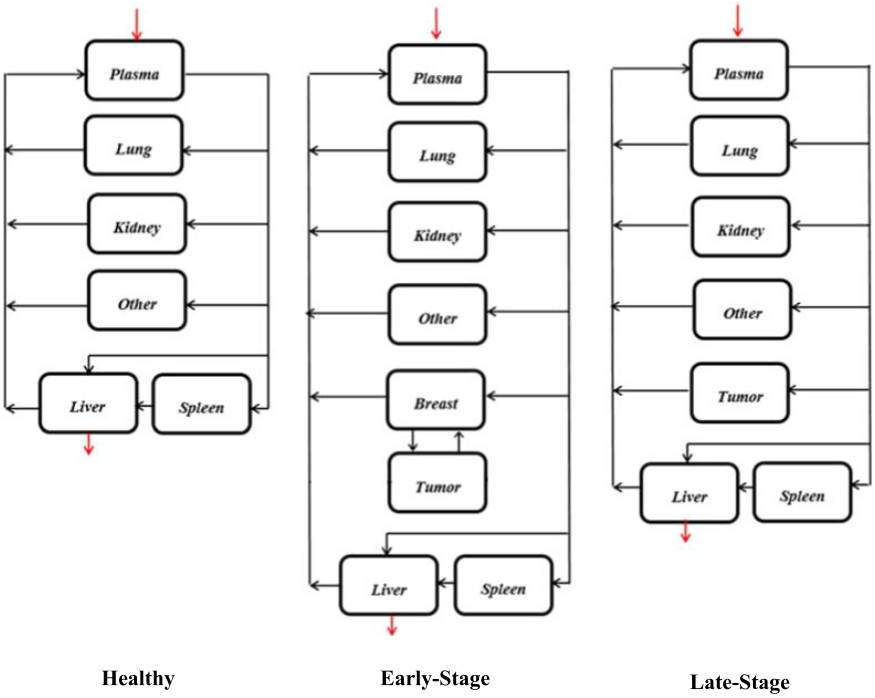

Figure 1 Physiologically-based pharmacokinetic connectivity for healthy, nontumor case (left), early-stage tumor (middle), and late-stage tumor (right).

tank reactor that is well mixed and perfusion limited. The well-mixed assumption states that each organ or tissue region is homogeneous, with immediate mixing such that the inlet flow concentration instantaneously equilibrates with the concentration in the tank and efflux. The ubiquity of capillaries in the body and the well-defined uniform exchange of QDs across these capillaries validate this assumption. Furthermore, the interstitial spaces of most organs tend to be uniform such that the concentration of substances entering/exiting the bloodstream is the same across the organ. Because the blood stream contains uniformly mixed QDs, the organs do as well, each according to their diffusion and perfusion properties. The perfusion-limited (or flow-limited) assumption states that diffusion is limited by regional blood flow into the capillaries of an organ or tissue. A corollary from this is that tissue membranes offer no significant resistance to molecular flow relative to the blood flow; diffusion across any membrane is very fast compared with blood transport. The perfusion-limited assumption is akin to the quasi-steady-state approximation used in chemical engineering kinetics. This is a valid assumption based on the small size of CalQDs and minimal interactions with the tissue membranes.[11]

Parameter selection

The main parameters of interest to construct this PBPK model are the physiological parameters of our organism of interest, the biophysical behavior of our substance of interest, and the interactions between the two in the form of partition coefficients. Fixed parameters of this model are compartment volumes and volumetric flowrates, whereas partition coefficients were varied among the healthy, early-stage, and late-stage models.

Organ masses can be found in literature for a multitude of organs and organisms as a fraction of body weight (BW).[16,17] Schaefer *et al*.[10] used female mice between the ages of 13–16 weeks, which have a mass of ~ 22.0 g.[16,17] Knowing the BW of the mouse, organ masses can be determined using the mean percent BW of each organ. From organ masses, organ volumes can be determined via the specific gravity of each organ. For the majority of organs or tissue regions, a specific gravity of 1.0 can be assumed as they are generally in this range (1.02–1.06) because they are composed primarily of water.[15,18] There are a few notable exceptions: marrow-free bone has a density of 1.92 g/cm^3, and the density of adipose tissue in mice is 0.916 cm^3/100 g BW. To determine the mass of adipose in a mouse, the following equation can be used[19]:

$$(\%\mathrm{BW}) = 0.0199(\mathrm{BW}) + 1.664 \quad (1)$$

Excluding the adipose and bone, the rest of the "other" compartment volume was determined using a specific gravity of 1.0. These three were then added for the lumped "other" compartment. Compartmental volumes for the model are shown in **Table 1**.

For a 22.0-g mouse with late-stage IBC, we used the tumor measurement given by Schaefer *et al*.[10] This value was also used to approximate the early-stage tumor—a small error considering the small size of the tumor—whereas the breast tissue BW was based on the weight of mammary glands reported by Fisher *et al*.[20] In the early-stage model, the breast compartment was created

Table 1 Compartmental volume and blood plasma volumetric flow rate parameters

Compartment	Volume (mL)	Volumetric flow rate (mL/hour)
Blood plasma	1.078	944.3
Lungs	0.1606	4.713
Kidneys	0.3674	85.77
Spleen	0.077 (0.154)	18.85
Liver	1.208	132.9
Breast	1.05	22.79
Tumor	0.08	1.766
Other	55.76	677.5

Compartmental volumes and volumetric flowrates were calculated from literature for a 22-g mouse.[14,15] The volume of the enlarged spleen case is shown in parenthesis. The tumor compartment volume and blood plasma flow rate were kept the same between the early-stage and late-stage models, so the values are an overestimate for the early-stage model.

by subtracting the volume for the breast tissue from the "other" organ compartment while maintaining a constant volume for the other organs.

The blood flow rate to each tissue region is given as a fraction of total cardiac output. The total cardiac output for our 22.0 g female mouse can be estimated from the following equation where BW is given in kilograms[19]:

$$\text{Cardiac output (L/min)} = 0.275(\text{BW})^{0.75} \quad (2)$$

From the mean percent cardiac outputs, blood flow to each organ can be determined. Additionally, the flow rate to the tumor is based on previously measured tumor blood flow rate scaled to our tumor size.[21] Compartmental volumetric flow rates are shown in **Table 1**.

QDs are injected intravenously into the organism, so the input to the model is a pulse into the plasma compartment. Effectively, this behaves as the plasma compartment starting with an initial concentration based on the dosage and distributing to the rest of the body as time progresses. The sink for QDs is from the liver compartment as biliary excretion, which takes the form of a first-order kinetic degradation of concentration with time. The following estimation for the first-order clearance rate constant was previously validated from experimental data for QD 705.[14] The value is very small because QD clearance from the body is slow with significant concentrations still measured even 28 days after intravenous injection.

$$k_{\text{elim}} = 1.0 \times 10^{-6}\,\text{hr}^{-1} \quad (3)$$

A partition coefficient is the equilibrium tissue-to-blood partition coefficient, a proportionality constant relating the tissue concentration of a substance *X* to the outgoing venous concentration. In the perfusion-limited case, it describes the ratio of the total tissue concentration of a substance *X* to its concentration in the outgoing blood flow. In practice, partition coefficients are approximated by the empirical equilibrium partition coefficient, which effectively lumps all processes that alter tissue extraction together in one term and is estimated experimentally using *in vitro* experimentation.[18] Due to the novelty of the QDs in this model, experimental partition coefficients do not yet exist, so estimation will be used going forward based on measured QD intensities (**Table 2**).[10,11]

Some partition coefficients are available for a similar QD (**Table S1**)[14]; assuming that conjugating calcitriol to QDs does not significantly affect the distribution of QDs in tissue we can use these values as a starting point. The initial partition coefficient estimates for the tumor compartment were based on the QD in question, with a low value used for the untargeted QDs and a much higher value used for targeted QDs, to consider the preferential attraction of SM3 CalQDs to IBC tumor cells that is expected due to the conjugated SM3 MUC1 antibodies.[10]

System of equations

The equations for the compartments are mass flow balances across homogeneous, well-stirred tissues with influx and efflux. Blood flows at the same volumetric flow rate, Q,

Table 2 Mean pixel intensity of QDs in organs of mice with no tumor and with late-stage tumor

		No tumor		Late-stage tumor	
QD	Organ	Intensity	Error (%)	Intensity	Error (%)
ConQD	Kidney	10.40	10.22	12.54	17.52
	Liver	16.23	22.20	14.85	16.91
	Lung	4.66	16.21	8.22	2.24
	Spleen	12.73	9.08	26.43	11.21
CalQD	Kidney	11.01	9.14	15.15	20.58
	Liver	20.38	12.99	20.15	31.96
	Lung	3.16	8.07	7.59	5.27
	Spleen	10.99	10.45	21.46	20.06
SM3 CalQD	Kidney	10.47	12.67	11.57	17.98
	Liver	17.18	6.91	18.12	8.22
	Lung	5.01	16.57	7.46	12.94
	Spleen	9.87	11.70	17.92	8.14

CalQD, calcitriol quantum dot; ConQD, control (unconjugated) QD; SM3, Mucin-3 antibodies; QDs, quantum dots.
Mice with and without SUM149 inflammatory breast cancer tumors were injected with SM3 CalQDs, CalQDs, or ConQDs, and after 4 days florescent images were taken. The mean pixel intensity values were reproduced with this model by fitting partition coefficient values with a residual sum of squares minimization.[10] The intensities reported for the late-stage tumor were also used for the early-stage model.

into and out of each constant compartment volume, V. The change in concentration with respect to time, $\dot{C}$, is equivalent to the blood flow rate divided by the constant volume, all multiplied by the concentration gradient across the compartment. The gradient can be represented by the change in concentration of a substance in the inflow (arterial concentration) compared with the outflow (venous concentration) due to distribution into the tissue. Additionally, an organ may have a sink or source, which will be represented here as a rate, *R*. Overall, this gives Eq. 4 for a single organ system.

$$\dot{C} = \frac{Q}{V}(c_i - c_o) + R \tag{4}$$

Because we are interested in the concentration in the actual tissue rather than in the circulatory system, we will utilize the partition coefficient, *P*, the ratio of concentration of substance *X* in the tissue, *c*, to the incoming plasma concentration of substance *X*, c_o. For compartments connected to the plasma compartment, c_o is the venous concentration of the substance.

$$P = \frac{c}{c_o} \tag{5}$$

Substituting this into Eq. 4, we have the following equation to describe a single organ system:

$$\dot{C} = \frac{Q}{V}(c_i - \frac{c}{P}) + R \tag{6}$$

Thus, for our healthy, nontumor system, containing the kidneys, liver, lungs, spleen, and plasma, with pulse input and excretion from the liver following first-order kinetics, we have the following set of differential equations with conserved volumetric flowrate:

$$\dot{C}_{\text{plasma}(p)} = \left(\frac{1}{V_p}\right)\left\{\left[\left(\frac{Q_k C_k}{P_k}\right) + (Q_{li} + Q_s)\frac{C_{li}}{P_{li}} + \left(\frac{Q_l C_l}{P_l}\right) + \left(\frac{Q_o C_o}{P_o}\right)\right] - (Q_{\text{total}})C_p\right\} \tag{7}$$

$$Q_{\text{total}} = Q_{\text{kidney}} + Q_{\text{liver}} + Q_{\text{spleen}} + Q_{\text{lung}} + Q_{\text{other}} \tag{8}$$

$$\dot{C}_{\text{kidney}(k)} = \left(\frac{Q_k}{V_k}\right)\left[C_p - \frac{C_k}{P_k}\right] \tag{9}$$

$$\dot{C}_{\text{lung}(l)} = \left(\frac{Q_l}{V_l}\right)\left[C_b - \frac{C_l}{P_l}\right] \tag{10}$$

$$\dot{C}_{\text{spleen}(s)} = \left(\frac{Q_s}{V_s}\right)\left[C_p - \frac{C_s}{P_s}\right] \tag{11}$$

$$\dot{C}_{\text{liver}(li)} = \left(\frac{1}{V_{li}}\right)\left[Q_{li}C_p + Q_s\frac{C_s}{P_s} - (Q_{li} + Q_s)\frac{C_{li}}{P_{li}} - kC_{li}\right] \tag{12}$$

$$\dot{C}_{\text{other}(o)} = \left(\frac{Q_o}{V_o}\right)\left[C_p - \frac{C_o}{P_o}\right] \tag{13}$$

For the late-stage IBC case, the blood plasma compartmental balance and overall molar flow equations change, as well as the addition of a tumor equation. All other equations remain the same.

$$\dot{C}_{\text{plasma}(p)} = \left(\frac{1}{V_p}\right)\left\{\left[\left(\frac{Q_k C_k}{P_k}\right) + (Q_{li} + Q_s)\frac{C_{li}}{P_{li}} + \left(\frac{Q_l C_l}{P_l}\right) + \left(\frac{Q_o C_o}{P_o}\right) + \left(\frac{Q_t C_t}{P_t}\right)\right] - (Q_{\text{total}})C_p\right\} \tag{14}$$

$$Q_{\text{total}} = Q_{\text{kidney}} + Q_{\text{liver}} + Q_{\text{spleen}} + Q_{\text{lung}} + Q_{\text{other}} + Q_{\text{tumor}} \tag{15}$$

$$\dot{C}_{\text{tumor}(t)} = \left(\frac{Q_t}{V_t}\right)\left[C_p - \frac{C_t}{P}\right] \tag{16}$$

In the case with an early-stage tumor, the equations remain the same except for those pertaining to the tumor and blood. In addition, a breast compartment is added, making these equations as follows:

$$\dot{C}_{\text{plasma }(p)} = \left(\frac{1}{V_b}\right)\left\{\left[\left(\frac{Q_k C_k}{P_k}\right) + (Q_{li} + Q_s)\frac{C_{li}}{P_{li}} + \left(\frac{Q_l C_l}{P_l}\right) + \left(\frac{Q_o C_o}{P_o}\right) + \left(\frac{Q_{\text{br}} C_{\text{br}}}{P_{\text{br}}}\right)\right] - (Q_{\text{total}})C_b\right\} \tag{17}$$

$$Q_{\text{total}} = Q_{\text{kidney}} + Q_{\text{liver}} + Q_{\text{spleen}} + Q_{\text{lung}} + Q_{\text{other}} + Q_{\text{breast}} \tag{18}$$

$$\dot{C}_{\text{breast }(\text{br})} = \left(\frac{1}{V_{\text{br}}}\right)\left[C_p Q_{\text{br}} + \frac{C_t Q_t}{P_t} - C_{\text{br}} Q_t - \frac{C_{\text{br}} Q_{br}}{P_{\text{br}}}\right] \tag{19}$$

$$\dot{C}_{\text{tumor}(t)} = \left(\frac{Q_t}{V_t}\right)\left[C_{\text{br}} - \frac{C_t}{P_t}\right] \tag{20}$$

Equations were solved simultaneously using the built-in function ode23s on MATLAB R2017b. All above parameters were constants found in literature except for the partition coefficients, which were varied from their original estimations such that model results match experimental florescence data 4 days after dosage in **Table 2** via a residual sum of squares minimization. As there are no fluorescence data available for mice with early-stage IBC, the data for the late-stage model are used. This results in significant error as the difference between the early-stage and late-stage models is only the change in connectivity. In the unhealthy, tumor cases, the model estimates the concentration of QDs in tumor tissue as well. In addition, the effect of doubling the volume of the spleen on the organ partition coefficients and model results was analyzed. Although we will look at an increased spleen volume, we maintain the spleen blood flow rates.

RESULTS

Partition coefficients

There is a lack of experimental information available on the QDs in question as the proposed treatment is a recent and novel development. The QDs have been found to accumulate in specific tissues,[8,10,12] so the partition coefficient for the "other" compartment was assumed to be 1. For all additional compartments, the partition coefficients

Table 3 Compartmental partition coefficient values for the three models

	No tumor			Early-stage tumor			Late-stage tumor		
Compartment	**ConQD**	**CalQD**	**SM3 CalQD**	**ConQD**	**CalQD**	**SM3 CalQD**	**ConQD**	**CalQD**	**SM3 CalQD**
Kidney	32.7	46.9	34.8	45.1	91.2	59.1	41.7	74.1	46.6
Liver	50.9	86.3	56.8	53.4	121.2	92.6	49.3	98.3	72.8
Spleen	40.0	46.9	32.8	95.0	129.1	91.5	88.0	105.0	72.3
Lung	14.6	13.4	16.6	29.6	45.7	38.1	27.3	37.1	30.1
Tumor	—	—	—	28.6	45.5	97.4	24.9	23.8	98.1
Breast	—	—	—	2.67	1.71	1.83	—	—	—

CalQD, calcitriol quantum dot; ConQD, control (unconjugated) QD; SM3, Mucin-3 antibodies.
Partition coefficients were found through a residual sum of squares minimization with experimental QD concentration data. The partition coefficient for the other compartment for each model was assumed to be 1.

used for each model are shown in **Table 3**, with the values for the enlarged spleen case shown in **Table S2**. In each case, tumor partition coefficients are much higher for the SM3 CalQDs compared with the untargeted QDs. However, tumor compartment partition coefficients are significantly sensitive to the initial estimate used as the compartmental volume is very small and the experimental concentration in the cancer cells for each is unknown. Additionally, partition coefficients for the kidney, liver, spleen, and lung compartments all increase under the enlarged spleen case. For SM3 CalQDs, this led to a lower concentration in the tumor compartment, especially for the early-stage case.

Model results

Normalized time-concentration graphs for SM3 CalQDs for each model (no tumor, early-stage tumor, and late-stage tumor) are shown in **Figure 2**. The maximum concentration of SM3 CalQDs in the tumor compartment is ~ 20% higher for the late-stage model than the early-stage. Additional plots for untargeted CalQDs and unconjugated control QDs (ConQDs) are in **Figures S1 and S2**. **Figure S3** is a reproduction of **Figure 2** extended to 4 days. These results show a very fast convergence to a steady concentration in each compartment except the tumor, which has a slower increase due to the relatively small blood plasma flow rate to the compartment. In the early-stage case, the breast compartment QD concentration remains low in comparison with the tumor compartment due to the large disparity in their partition coefficients and relatively small size of the tumor compartment. QD concentrations in the spleen and kidneys quickly peak before decreasing and redistributing some of the QDs to other compartments. Other tissue regions exhibit a monotonic increase over the entire time span.

In **Figure 3**, QD concentration profiles in the spleen compartment for the normal and enlarged spleen cases are compared in the late-stage model. The enlarged spleen volume is used as an example of a potential application of the model to describe changes in QD distribution due to a common symptom of cancer. Of note is the loss of an initial peak before reaching a relatively steady-state value; this behavior represents a relative loss in blood flow to the spleen. These dynamics are mirrored in the early-stage case. Other compartmental time-concentration profiles are qualitatively unaffected by spleen volume.

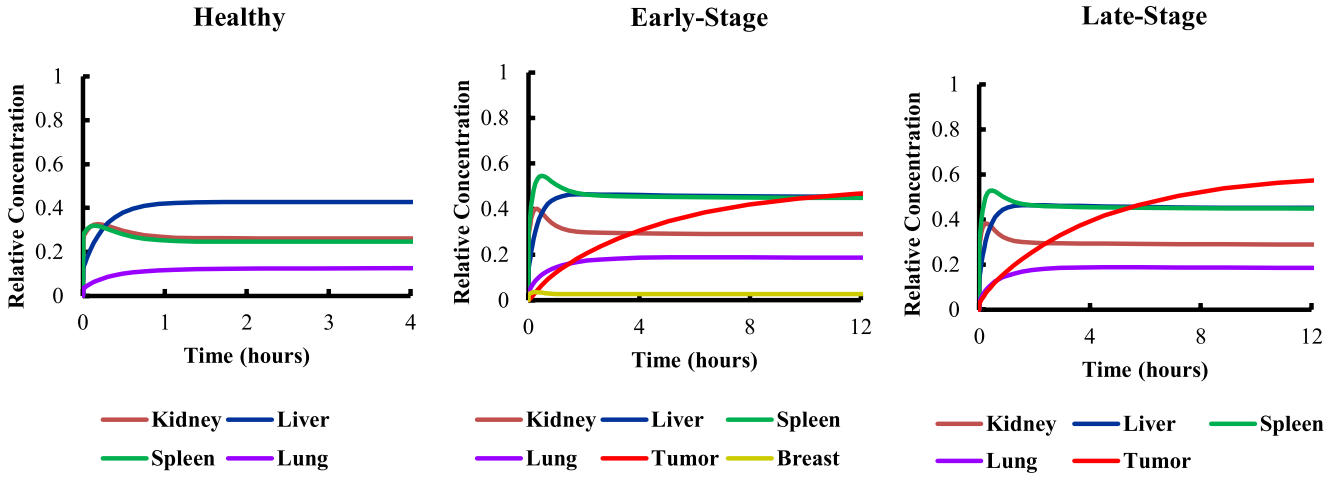

Figure 2. SM3 calcitriol quantum dot healthy (left), early-stage (middle), and late-stage (right) time-concentration results for regular spleen size. Concentration values are normalized by the initial concentration in the plasma compartment. The results are shown only to 4 or 12 hours, as concentrations afterward are steady state and scaling the figure would obscure these dynamics. SM3, Mucin-3 antibodies.

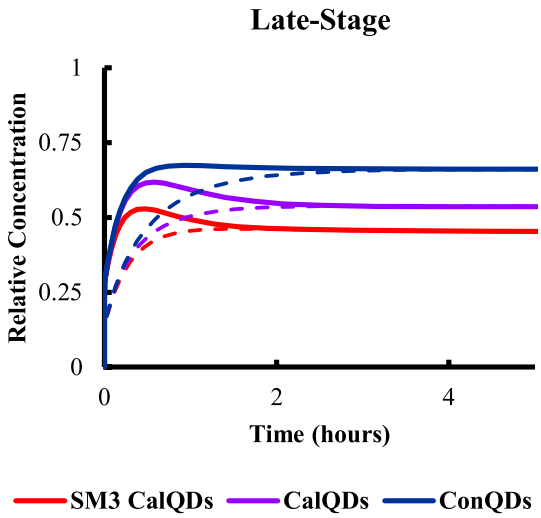

Figure 3 Late-stage spleen compartment concentration for SM3 calcitriol quantum dots (CalQDs; red), CalQDs (purple), and ConQDs (blue) with corresponding enlarged spleen results (dotted). Results for the early-stage model are similar. Concentration values are normalized by the initial concentration in the plasma compartment. ConQD, control (unconjugated) QD; SM3, Mucin-3 antibodies.

DISCUSSION

Overall, it was shown that a PBPK model can be used to describe the behavior and distribution of QDs both in healthy and tumorous mice. Although partition coefficient data for any of the QDs in question are unavailable, estimated partition coefficients were found that produced simulated data consistent with that found experimentally. This model generates continuous time-concentration data of QDs in several tissue regions, which can be useful for quantifying short-term and long-term behavior of the various QDs in each tissue region.

In all simulations, no QD concentration exceeds the initial dosage, so hypercalcemia due to extreme local concentrations should not be a concern. However, changes such as experimentally determined partition coefficients or more aggressive dosing regimens could lead to larger spikes in compartmental QD concentration. Of special interest are maximum QD concentrations in the spleen, liver, and kidneys because these organs are richly perfused and have been shown to accumulate QDs in mice.[8,10,12] Toxic tissue concentration of QDs could remain excessive for weeks, so it is important to be able to predict and prevent this.

When partition coefficients are estimated with experimental tissue concentration data, any partition coefficient not explicitly validated by the data will cause significant error in the resulting time-concentration values. In this case, assuming the "other" compartment has a partition coefficient of 1 is a substantial source of error, as the compartment is most of the volume in the system and receives over two-thirds of the total blood flow. This error is easily observable due to the large differences between the partition coefficients in **Table 3** for the same organ. In this way, the partition coefficients reported are empirical and cannot be deconvoluted to find the true physiological partition coefficient. Thus, interpretation of a larger partition coefficient for a different QD or different model as meaning a higher affinity for the given QD is only true within each instance of the simulation. That is, only the relationship between partition coefficients for each compartment in a given model can be considered. In particular, the tumor compartment partition coefficient is quite variable and cannot be determined with much certainty without further information. Moreover, the experimental QD concentration measurements used to fit the partition coefficients may contain errors whose effects cannot be accounted for in a straightforward manner. Not enough data exist to determine standard error at this time; as more experimental data become available, adjustments can be made to this framework.

For this model to be quantitatively predictive, further experimental data are needed to estimate the partition coefficients. The best option is conducting *in vitro* experiments to determine physiological partition coefficients[22] so that the model could be developed fully *a priori* rather than based on experimental concentration data. Currently, the model presented is limited because the data used to estimate the partition coefficients do not contain information about the short-time dynamics of QD distribution. The data are for QD concentration 4 days after dosage, yet, in this model, most dynamics happen on the time scale of hours. This error is seen in the results, where QD concentrations peak earlier than during the second day, as observed by Schaefer *et al*.[10]

A valuable improvement to this model is the incorporation of the lymphatic system, which plays an important role in IBC. In addition to blood flow, the model would include lymph flow that comes from each compartment, goes through a lymph node compartment, and is emptied into venous blood. IBC tumor emboli often travel through dermal lymphatic vessels causing distant metastases.[3] Symptoms are typically observed after the initial tumor has metastasized, so it is valuable to consider the lymphatic system as it is systematically interconnected with the network of metastases. In addition, decoupling distribution by blood flow and lymph flow would help explain the preference of QDs to organs that are heavily involved in lymph flow (e.g., lungs) in tumorous mice, even in the case of untargeted QDs.[10] Furthermore, the model could consider tumor metastasis with the addition of a tumor subcompartment for each tissue and delumping tissues particularly susceptible to metastasis from the "other" compartment like bone and skin. Then, tumor emboli could be represented by concentration in blood and lymph. More ambitiously, the presence of agents other than calcitriol that affect IBC cells, such as TGFβ, which plays a role in IBC emboli formation as well as IBC cell clustering during movement through the body, could supplement this tumor metastasis model.[3] Expanding the model in this way allows for real-time quantitative simulation of IBC treatment, with tumor growth and QD distribution occurring simultaneously.

Progress in understanding disease on the molecular level has led to an increased popularity of personalized medicine, a strategy where treatment depends on models that characterize and differentiate patients based on their individual characteristics. The classic trial-and-error approach to treating disease has many shortcomings, notably that the physician or experimentalist must make an educated guess about which treatment will

be most effective, as well as when to administer it and how much to give the patient. Allometric scaling of the compartment volumes can be used to adapt this model for use in predicting appropriate dosages for clinical or experimental trials with QD IBC treatments on other animals.[23] Adaptation of this model for humans should be accompanied by specific emphasis placed on accurate modeling of the breast compartment. Currently, the model lacks enough experimental data to provide reliable QD concentration estimates. However, further experimental validation of the model would allow for dynamic quantitative prediction of QD concentrations, which when coupled with a well-developed therapy program could be a powerful tool for fighting IBC. For instance, the model can be used to determine peak concentrations as well as area under the curve (AUC) exposures, which are crucial factors in designing chemotherapy regimens and dosing schedules. This translates to prediction of the optimal SM3 CalQD dosage amount and frequency to provide a target exposure of the QDs based on how developed the IBC is, while avoiding hypercalcemia in other tissues.

This PBPK model has been constructed and validated for multiple QDs, notably SM3 CalQDs, which are of interest for IBC treatment. SM3 CalQDs provide a targeted calcitriol treatment for IBC cells, which is important to mitigate cancerous effects of the tumor cells while allowing for live cell direct imaging and avoiding hypercalcemia in patients. Further *in vitro* analysis of the QDs is recommended so that currently estimated parameters can be replaced by physiologically accurate values to complete the top-down model. This model has potential as a predictive tool to guide or supplement both experimental and clinical endeavors in QD treatment of IBC with the hope that a more successful treatment is developed.

Supporting Information. Supplementary information accompanies this paper on the *Clinical and Translational Science* website (www.cts-journal.com).

Figure S1. Time-concentration graphs for CalQDs.
Figure S2. Time-concentration graphs for ConQDs.
Figure S3. Four-day time-concentration graphs for SM3 CalQDs.
Table S1. Initial guesses for model partition coefficients.
Table S2. Compartmental partition coefficient values for each model with an enlarged spleen volume.
Model Code

Acknowledgments. Preliminary developments on this project were made by Bikram Paul and Melanie Salinas.

Funding. No funding was received for this work.

Conflict of Interest. The authors declared no competing interests for this work.

Author Contributions. J.F., M.S., M.W., J.G., A.N., and P.S. wrote the manuscript. J.F., M.S., M.W., R.S., J.G., A.N., and P.S. designed the research. J.F., M.S., M.W., R.S., and K.vG. performed the research. J.F., M.S., and M.W. analyzed the data.

1. Barkataki, S., Javadekar, M.J., Bradfield, P., Murphy, T., Witmer, D.D. & Van Golen, K.L. Inflammatory breast cancer: a panoramic overview. *J. Rare Dis. Res. Treat.* **3**, 37–43 (2018).
2. Robertson, F.M. *et al.* Inflammatory breast cancer: the disease, the biology, the treatment. *CA Cancer J. Clin.* **60**, 351–375 (2010).
3. Lehman, H.L. *et al.* Modeling and characterization of inflammatory breast cancer emboli grown *in vitro. Int. J. Cancer* **132**, 2283–2294 (2013).
4. Berman, A.T., Thukral, A.D., Hwang, W., Solin, L.J. & Vapiwala, N. Incidence and patterns of distant metastases for patients with early-stage breast cancer after breast conservation treatment. *Clin. Breast Cancer* **13**, 88–94 (2013).
5. Krathen, R.A., Orengo, I.F. & Rosen, T. Cutaneous metastasis: a meta-analysis of data. *South. Med. J.* **96**, 164–167 (2003).
6. House Call: Vitamin D and Cancer Prevention. MD Anderson Cancer Center. <https://www.mdanderson.org/publications/oncolog/October-2016/vitamin-d-and-cancer-prevention.html> (2016). Accessed December 16, 2018.
7. Lehmann, B. & Meurer, M. Vitamin D metabolism. *Dermatol. Ther.* **23**, 2–12 (2010).
8. Beer, T.M. & Myrthue, A. Calcitriol in cancer treatment: from the lab to the clinic. *Mol. Cancer Ther.* **3**, 373–381 (2004).
9. Hillyer, R.L., Sirinvasin, P., Joglekar, M., Sikes, R.A., van Golen, K.L. & Nohe, A.G. Differential effects of vitamin D treatment on inflammatory and non-inflammatory breast cancer cell lines. *Clin. Exp. Metastasis* **8**, 971–979 (2012).
10. Schaefer, R.J., Russell, R., Akkiraju, H., Bonor, J.C., van Golen, K.L. & Nohe, A.G. Targeting of calcitriol to inflammatory breast cancer tumors and metastasis *in vitro* and *in vivo. Biol. Syst.* **1**, 104 (2012).
11. Schaefer, R.J. Calcitriol conjugated quantum dots, an innovative tool as both probe and treatment. University of Delaware Master's Thesis (2012).
12. Breslau, N.A., McGuire, J.L., Zerwekh, J.E., Frenkel, E.P. & Pak, C.Y. Hypercalcemia associated with increased serum calcitriol levels in three patients with lymphoma. *Ann. Intern. Med.* **100**, 1–7 (1984).
13. Lv, Y. *et al.* Hypersplenism: history and current status. *Exp. Ther. Med.* **12**, 2377–2382 (2016).
14. Lin, P. *et al.* Computational and ultrastructural toxicology of a nanoparticle, quantum dot 705, in mice. *Environ. Sci. Technol.* **42**, 6264–6270 (2008).
15. Li, M., Al-Jamal, K.T., Kostarelos, K. & Reineke, J. Physiologically based pharmacokinetic modeling of nanoparticles. *ACS Nano* **4**, 6303–6317 (2010).
16. Body Weight Information for C57BL/6J. The Jackson Laboratory. <https://www.jax.org/jax-mice-and-services/strain-data-sheet-pages/body-weight-chart-000664#> (2018). Accessed December 16, 2018
17. Rat and Mice Weights. Animal Resources Centre. <http://www.arc.wa.gov.au/?page_xml:id=125> (2018). Accessed December 16, 2018.
18. DiStefano, J. Dynamic Systems Biology Modeling and Simulation, 1st edn. (Elsevier, Amsterdam, UK, 2013).
19. Brown, R.P., Delp, M.D., Lindstedt, S.L., Rhomberg, L.R. & Beliles, R.P. Physiological parameter values for physiologically based pharmacokinetic models. *Toxicol. Ind. Health* **13**, 407–484 (1997).
20. Fisher, J.W., Whittaker, T.A., Taylor, D.H., Clewell, H.J. & Andersen, M.E. Physiologically based pharmacokinetic modeling of the lactating rat and nursing pup: a multiroute exposure model for trichloroethylene and its metabolite, trichloroacetic acid. *Toxicol. Appl. Pharmacol.* **102**, 497–513 (1990).
21. Sakaeda, T., Fukumura, K., Takahaski, K., Matsumura, S., Matsuura, E. & Hirano, K. Blood flow rate in normal and tumor-bearing rats in conscious state, under urethane anesthesia, and during systemic hypothermia. *J. Drug Target.* **6**, 261–272 (1998).
22. Crowell, S.R., Henderson, W.M., Fenneke, J.F. & Fisher, J.W. Development and application of a physiologically based pharmacokinetic model for triadimefon and its metabolite triadimenol in rats and humans. *Toxicol. Lett.* **205**, 154–162 (2011).
23. Sharma, V. & McNeil, J.H. To scale or not to scale: the principles of dose extrapolation. *Br. J. Pharmacol.* **157**, 907–921 (2009).